



Universiteit
Leiden
The Netherlands

The relation between the mass accretion rate and the disk mass in Class I Protostars

Fiorellino, E.; Tychoniec, Ł.; Manara, C.F.; Rosotti, G.P.; Antonucci, S.; Miera, F.C.-S. de; ... ; Nisini, B.

Citation

Fiorellino, E., Tychoniec, Ł., Manara, C. F., Rosotti, G. P., Antonucci, S., Miera, F. C. -S. de, ... Nisini, B. (2022). The relation between the mass accretion rate and the disk mass in Class I Protostars. *Astrophysical Journal Letters*, 937(1). doi:10.3847/2041-8213/ac8fee

Version: Publisher's Version
License: [Creative Commons CC BY 4.0 license](https://creativecommons.org/licenses/by/4.0/)
Downloaded from: <https://hdl.handle.net/1887/3561742>

Note: To cite this publication please use the final published version (if applicable).



The Relation between the Mass Accretion Rate and the Disk Mass in Class I Protostars

Eleonora Fiorellino^{1,2,3} , Łukasz Tychoniec⁴ , Carlo F. Manara⁴ , Giovanni Rosotti^{5,6} , Simone Antoniucci⁷ ,
Fernando Cruz-Sáenz de Miera^{1,2} , Ágnes Kóspál^{1,2,8,9} , and Brunella Nisini⁷

¹ Konkoly Observatory, Research Centre for Astronomy and Earth Sciences, Eötvös Loránd Research Network (ELKH), Konkoly-Thege Miklós út 15-17, 1121 Budapest, Hungary

² CSFK, MTA Centre of Excellence, Budapest, Konkoly Thege Miklós út 15-17., H-1121, Hungary

³ INAF-Osservatorio Astronomico di Capodimonte, via Moiariello 16, I-80131 Napoli, Italy

⁴ European Southern Observatory, Karl-Schwarzschild-Strasse 2, D-85748 Garching bei München, Germany

⁵ Leiden Observatory, Leiden University, PO Box 9513, NL-2300 RA Leiden, The Netherlands

⁶ School of Physics and Astronomy, University of Leicester, University Road, Leicester, LE1 7RH, UK

⁷ INAF-Osservatorio Astronomico di Roma, via di Frascati 33, I-00078, Monte Porzio Catone, Italy

⁸ Max Planck Institute for Astronomy, Königstuhl 17, D-69117 Heidelberg, Germany

⁹ ELTE Eötvös Loránd University, Institute of Physics, Pázmány Péter sétány 1/A, 1117 Budapest, Hungary
Received 2022 July 29; revised 2022 September 5; accepted 2022 September 7; published 2022 September 21

Abstract

Evidence of a relation between the mass accretion rate and the disk mass is established for young, Class II pre-main-sequence stars. This observational result opened an avenue to test theoretical models and constrain the initial conditions of disk formation, fundamental in the understanding of the emergence of planetary systems. However, it is becoming clear that planet formation starts even before the Class II stage, in disks around Class 0 and I protostars. We show for the first time evidence for a correlation between the mass accretion rate and the disk mass for a large sample of Class I young stars located in nearby (<500 pc) star-forming regions. We fit our sample, finding that the Class I object relation has a slope flatter than Class II stars, and the former have higher mass accretion rates and disk masses. The results are put in context of disk evolution models.

Unified Astronomy Thesaurus concepts: [Star formation \(1569\)](#); [Stellar accretion disks \(1579\)](#); [Protostars \(1302\)](#); [Low mass stars \(2050\)](#); [Planet formation \(1241\)](#); [Circumstellar disks \(235\)](#); [Circumstellar dust \(236\)](#)

1. Introduction

Young stellar objects (YSOs) evolve as the result of a complex interplay between the forming star, the circumstellar disk, where planet formation occurs, and the envelope. Modeling efforts to describe such intricate interplay span all ranges of the protostellar lifetime from pre-stellar cores to non-accreting young stars. However, comparisons of theoretical predictions with observations of stellar properties are limited to the well-characterized Class II disks of the pre-main-sequence (PMS) phase (Manara et al. 2022, and references therein).

Observations of the Class 0/I stages are especially important in the context of constraining the initial conditions for models of disk evolution. In particular, a fundamental parameter which describes part of this interplay is the mass accretion rate (\dot{M}_{acc}) which correlates with the disk mass (M_{disk}). This correlation was predicted by viscous models (Hartmann et al. 1998), and recently confirmed by observations (Manara et al. 2016) for Class II objects.

Since the advent of submillimeter interferometry and complete surveys of planet-forming disks, our knowledge of the disks around the youngest protostars has greatly expanded (Sheehan & Eisner 2017; Maury et al. 2019; Williams et al. 2019; Tobin et al. 2020; Tychoniec et al. 2020; Miotello et al. 2022). At the same time, thanks to new infrared (IR) facilities, some efforts to characterize the stellar properties of the youngest stars (e.g., Fiorellino et al. 2021; Laos et al. 2021)

as well as available archival observations (Muzerolle et al. 1998; White & Hillenbrand 2004; Doppmann et al. 2005; Connelley & Greene 2010) have shown a promising way to investigate \dot{M}_{acc} in the protostellar phase.

In this letter we put recent observations of Class I protostars in the context of disk evolution models, both in the viscous and disk wind paradigms (Lodato et al. 2017; Tabone et al. 2021), and models of early stages of core collapse and disk formation (Hennebelle et al. 2020; Zhao et al. 2020). We present and discuss the \dot{M}_{acc} versus M_{disk} relation for the first time for Class I protostars.

2. Sample & Method

This work is based on already existing observations of protostellar sources. The sample analysed here is composed of 26 Class I young stars (whose spectral index between 2 and 24 μm is $\alpha > -0.3$, i.e., we include also flat spectrum objects) located within 500 pc of the Sun. The choice of these sources is driven by the need for a homogeneous computation of the mass accretion rate and the disk mass. Therefore, we collect sources whose accretion analysis is based on near-IR (NIR) spectroscopic tracers, and using millimeter archival data we calculate the disk dust mass. These criteria were satisfied by three objects observed by Nisini et al. (2005a) in the Corona Australis cloud, three objects from Antoniucci et al. (2008), all within 450 pc, six objects out of the 10 analysed by Fiorellino et al. (2021) in the NGC 1333 cluster in the Perseus star-forming region, and 14 objects from E. Fiorellino et al. (submitted) out of the 40 protostars analysed therein. The list of targets included in the analysis is reported in the [Appendix](#).

2.1. The Mass Accretion Rate

The mass accretion rate for all these sources was computed by using similar methods that provide comparable results. The main common assumption is that the accretion during the Class I stage can be described through the magnetospheric accretion scenario (for a recent review, see Hartmann et al. 2016) and computed with the related equation:

$$\dot{M}_{\text{acc}} \sim \left(1 - \frac{R_{\star}}{R_{\text{in}}}\right)^{-1} \frac{L_{\text{acc}} R_{\star}}{GM_{\star}}, \quad (1)$$

where R_{in} is the inner-disk radius, which we assume to be $R_{\text{in}} \sim 5 R_{\star}$ (Hartmann et al. 1998), and G is the gravitational constant. Nisini et al. (2005a) computed the accretion luminosity by the difference between the bolometric and the stellar luminosity. They found that their results for Class I protostars were in agreement with L_{acc} computed using empirical relations that link the HI emission lines, $Pa\beta$, and $Br\gamma$ with the accretion luminosity of Class II PMS stars from Muzerolle et al. (1998). Antonucci et al. (2008) derived accretion rates using a self-consistent method based on the aforementioned empirical relations, the assumption that the bolometric luminosity is the sum of the accretion and stellar luminosity ($L_{\text{bol}} = L_{\text{acc}} + L_{\star}$), the equation of the bolometric magnitude in the K band: $M_{\text{bol}} = BC_K + m_K + 2.5 \log(1 + r_K) - A_K - 5 \log(d/10\text{pc})$, and the assumption that these sources lie on the birthline (as described by Palla & Stahler 1990). Later on, Fiorellino et al. (2021) and E. Fiorellino et al. (submitted) adopted the same self-consistent method by using the most recent empirical relations of Alcalá et al. (2017) and assuming the age of these sources is between the birthline and 1 Myr, based on Spitzer-based lifetime estimates for Class I and flat objects (Enoch et al. 2009; Dunham et al. 2014). For a detailed description of the self-consistent method we refer the reader to Antonucci et al. (2008) and Fiorellino et al. (2021). The average error on the mass accretion rate is 0.8 dex (Fiorellino et al. 2021). However, we note that since young stars exhibit variability, a further 0.5 mag uncertainty in the flux (Lorenzetti et al. 2013) should be considered. This propagates to a variation on the flux of about 50%, enlarging the uncertainties on the \dot{M}_{acc} as a consequence.

We would like to focus the attention of the reader on the following observational limit. This kind of mass accretion analysis is possible only for sources where the IR veiling due to the disk and envelope is sufficiently low that we can see the photosphere. Usually, according to the current correspondence between classes based on the spectral energy distribution spectral index and evolutionary path, the less embedded objects are the more evolved ones. Therefore, we can consider this sample of Class I objects representative of the brightest and more evolved Class I protostars.

2.2. The Disk Dust Mass

For the overall sample we performed a coordinate and sources name search across the literature and also looked for archival interferometric data. We included a dust mass measurement in our analysis if the flux measurement was available at $<1''$ resolution. In the subarcsecond regime, where

the size of the beam is comparable to the disk size, the envelope contribution is usually negligible, especially for Class I systems where the envelope is largely dissipated (Tychoniec et al 2020). If there was no flux reported in the literature and data were available in the archive, we performed a 2D Gaussian fit to the continuum image to extract the flux density. This was done using pipeline-processed products from the archives, without any additional processing.

From the flux density (F_{ν}) we calculated the dust mass by inverting the modified blackbody equation:

$$M_{\text{dust}} = \frac{d^2 F_{\nu}}{\kappa_{\nu}(\beta) B_{\nu}(T_{\text{dust}})}, \quad (2)$$

where d is the distance to the source, B_{ν} is the Planck function for the dust temperature T_{dust} , and κ_{ν} is the dust opacity at the frequency of the observation ν . The disk mass (M_{disk}) is obtained from the dust mass assuming a typical dust-to-gas ratio of 1:100. Equation (2) is accurate for optically thin emission, otherwise it provides a lower limit on the dust mass measurement. An isothermal disk with $T = 30\text{K}$ is assumed, which is the temperature typically used for young, embedded disks. If the disks are colder, similar to the Class II systems, this would result in an increase of the total dust mass. The dust opacity value at 1.3 mm is $0.00899 \text{ g cm}^{-2}$, taken from Ossenkopf & Henning (1994), and for observations at different wavelengths the spectral emissivity is scaled with $\beta = 1$, which assumes some degree of grain growth (Natta et al. 2005). With these uniform assumptions on the dust properties we are not introducing any additional discrepancies between the disks measured by different observing projects. The accuracy of the disk mass estimation is a matter of ongoing debate (see Manara et al. 2022; Miotello et al. 2022 and references therein). Several studies point to severe underestimation of the disk mass due to optical thickness or dust scattering (Zhu et al. 2019). The recent work of Sheehan et al. (2022) shows that Class 0/I disk dust masses can be overestimated—especially on the low-mass end—if the simplistic assumption of an isothermal disk is used. Combined, these effects would result in increased spread of the disk masses (i.e., more massive disks would be even more massive while the low-mass end would have even lower masses).

3. Results and Discussion

Viscous models of disk evolution predict a strong correlation between \dot{M}_{acc} and M_{disk} (e.g., Hartmann et al. 1998; Dullemond et al. 2006; Rosotti et al. 2017). In the last years, this relation has been investigated in classical T Tauri star (CTTS) samples thanks to accurate measurements of the mass accretion rate and disk mass for several nearby ($<500 \text{ pc}$) star-forming regions (see Manara et al. 2022 and references therein). In brief, these works show that the predicted trend is confirmed by observations with a spread of about ~ 1 dex (Manara et al. 2016). Moreover, the spread is still present for old star-forming regions like Upper Scorpius (Manara et al. 2020). This is contrary to expectations of viscous models which predict a decrease of the spread with the age of the CTTS population. An interesting missing piece of information in this debate is whether the strong correlation is still valid in the earlier stages, where the viscous timescale starts to be comparable or larger

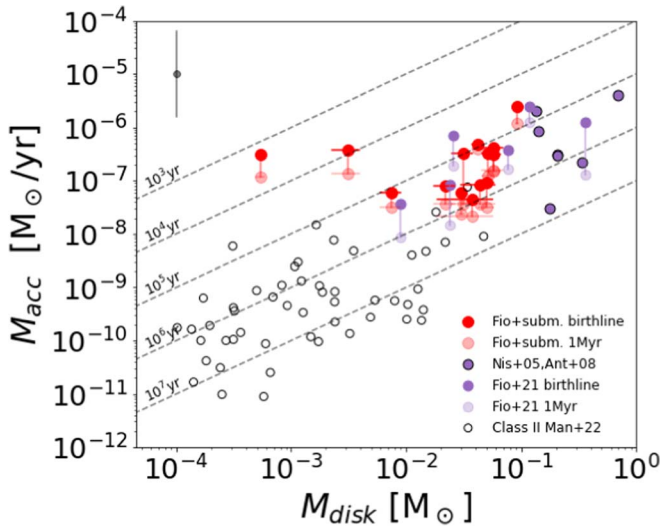


Figure 1. Mass accretion rate vs. disk dust mass. Red filled circles are the Class I sources where \dot{M}_{acc} is the mean value between the results assuming the birthline and 1 Myr old evolutionary track. The purple filled circles are other Class I sources from the literature. Empty circles are Class II objects from the Lupus sample. The black dashed lines correspond to several disk depletion times $t_d = \dot{M}_{\text{acc}}/M_{\text{disk}}$, from 10^3 yr (top) to 10^7 yr. A representative error bar for the mass accretion rate is shown in gray on the top left corner of the plot.

than the YSO lifetime itself. In particular, with information of the accretion rates and disk masses in the earlier stages of evolution we can constrain the initial conditions of the disk evolution models.

3.1. $\dot{M}_{\text{acc}}-M_{\text{disk}}$ in Class I Protostars

Figure 1 shows the mass accretion rate as a function of the total disk mass for our sample of Class I protostars. For each source, we plot the \dot{M}_{acc} derived assuming the sources are on the birthline and the one derived assuming they are 1 Myr old, which correspond to the limits of the possible values. We also plot Class II disks in Lupus, the properties of which were obtained by Manara et al. (2022), to provide a comparison of our sample with more evolved sources. Depletion times $t_d = \dot{M}_{\text{acc}}/M_{\text{disk}}$ from 10^3 yr to 10^7 yr are plotted (black dashed lines).

The plot shows that the more disk massive Class I systems are matching the trend seen for Class II disks in the Lupus star-forming region from Manara et al. (2016), with depletion times of 10^4 yr $< t_d < 10^7$ yr. An exception is represented by two protostars, ones with less massive disks, and the only two sources in the region of the \dot{M}_{acc} versus M_{disk} described by depletion times shorter than 10^4 yr. Considering the overall sample of Class I objects, there is large scatter in the \dot{M}_{acc} versus M_{disk} distribution. This trend is particularly notable for sources with $M_{\text{disk}} < 10^{-2} M_{\odot}$.

To investigate the relation between the Class I and II YSO samples, we performed a two-sample Kolmogorov–Smirnov test (KS test) to quantify the difference of their $M_{\text{disk}} - \dot{M}_{\text{acc}} - \text{yr}$ distributions. We obtained that the probability that the Class I and II samples could have been drawn from the same probability distribution is 0.2 considering Class I on the birthline, and 0.4 considering Class I being 1 Myr old. Assuming the two ages as “limits” for our sample, the probability that our sample of Class I YSOs is drawn from the same probability distribution as the Lupus Class II objects is $0.2 < p < 0.4$. We note that by assuming 1 Myr as the Class I

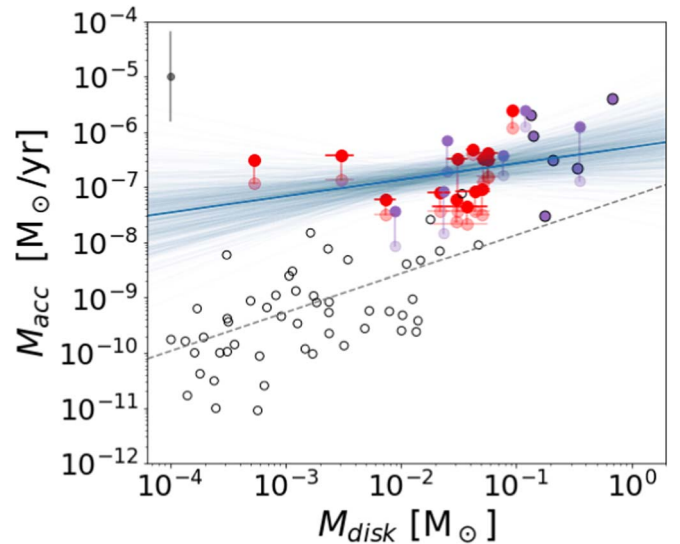


Figure 2. Mass accretion rate vs. disk dust mass. The symbols are the same as in Figure 1. The blue line corresponds to our best fit for the overall sample of Class I YSOs, while the light-blue lines show a subsample of the results of some chains. The dashed gray shows the best fit for the Class II YSOs (Manara et al. 2016).

sample age, the probability to have the same statistical distribution of Class II is not negligible. This result shows that the $M_{\text{disk}} - \dot{M}_{\text{acc}} - \text{yr}$ distributions can be separated depending on the evolutionary stage of the disk, evolving with the age. This can be due to a type of different evolution of the disk during the Class I stage, when refueling from the envelope is not negligible. Figure 1 also suggests that Class I disks accrete more material on the central star than Class II.

In Figure 2 we performed a linear regression fit of the Class I protostars sample (light-blue dashed line) considering the mean value of the \dot{M}_{acc} between the one computed assuming sources on the birthline and 1 Myr old, having as the error the standard deviation plus the intrinsic uncertainty. We used the hierarchical Bayesian method of Kelly (2007), which considers errors in both axes of the plot. We found the following relation $\log(\dot{M}_{\text{acc}}) = (0.3 \pm 0.2)\log(M_{\text{disk}}) + (-6.3 \pm 0.3)$ with a standard deviation of 0.4 ± 0.1 . We compare our fit with the one performed for Class II objects (Manara et al. 2016). The gray dashed line in Figure 2 shows the Class II slope of 0.7 ± 0.2 moved upwards in the plot, at the same intercept we obtained. Our best fit shows a slope flatter than the one obtained for Class II, lying always above the Class II sample. We note that if we remove from the fitted sample the two sources with the smallest disk masses, we find a slope of 1.1 ± 0.2 , compatible within the error with the Class II slope. This could suggest that to determine how and how much the Class I and II YSOs $\dot{M}_{\text{acc}} - M_{\text{disk}}$ distributions are different, we should analyse Class I objects with low disk masses, comparable with the disk mass typical of Class II sources, to verify whether these two sources are outliers or Class I sources show a flatter slope in general. On the other edge of the distribution, we expect that more embedded (and younger) protostars, with $M_{\text{dust}} > 20 M_{\oplus}$ (i.e., $M_{\text{disk}} > 6 \times 10^{-4} M_{\odot}$), would lay above the current distribution, i.e., higher \dot{M}_{acc} and similar M_{disk} , as suggested by the simulations of Hennebelle et al. (2020), which provide almost a constant value of about $1.5 \times 10^{-2} M_{\odot}$ for the protostellar disk mass until 0.16 Myr. In this case, it would be

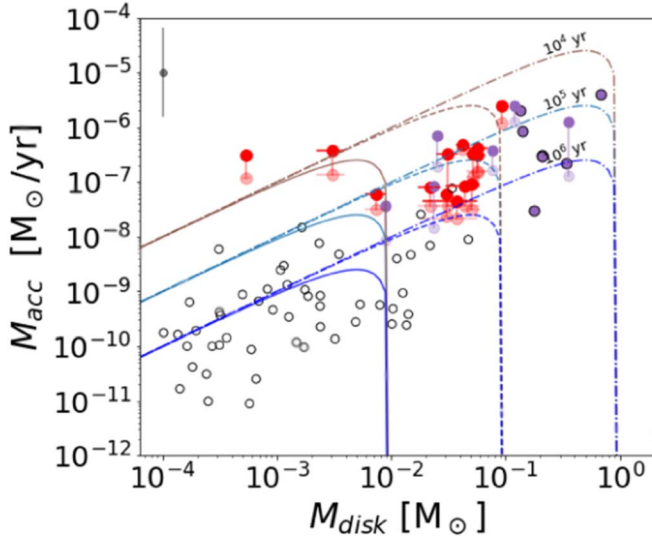


Figure 3. Mass accretion rate vs. disk dust mass. The symbols are the same as in Figure 1. The brown, light-blue, and blue dashed lines are isochrones from Lodato et al. (2017) at $t_\nu = 10^4$, 10^5 , and 10^6 yr, respectively. For each t_ν we show in solid, dashed, and dashed-dotted lines isochrones for three different initial disk masses (0.01, 0.1, and $1 M_\odot$, respectively).

possible to exclude the same evolutionary path (same slope) with different initial disk conditions.

Limiting our discussion to the Class I sample we analysed, we can state that they tend to have higher mass accretion rates when contrasted with Class II disks with a comparable disk mass, and that the $\dot{M}_{\text{acc}}-M_{\text{disk}}$ distribution is flatter in Class I than in Class II YSOs. This implies that, assuming M_{disk} and \dot{M}_{acc} constant within the Class I lifetime (~ 0.54 yr; Enoch et al. 2009; Dunham et al. 2014), the disk should be dissipated within 10^5-10^6 yr for most of the protostars in our sample. But we know that the presence of the disks in the YSO systems last until $\sim 10^6-10^7$ yr. Possible solutions to this discrepancy are: (1) \dot{M}_{acc} is not constant. For example, it can be possible that during this very short evolutionary stage, \dot{M}_{acc} decreases rapidly, reaching lower values typical of Class II objects, not totally dissipating the disk, and (2) \dot{M}_{acc} is constant during the Class I protostellar stage, but the disk is fueled by an “extra mass” coming from the envelope.

On one hand, we still have to collect suitable data to check predictions on the $\dot{M}_{\text{acc}}-M_{\text{disk}}$ distribution, which consider a continuous fuel of material from the envelope to the disk (i.e., Hueso & Guillot 2005); on the other hand, the scenario in which \dot{M}_{acc} decreases rapidly to conserve the disk is described by Lodato et al. (2017). To investigate this hypothesis, we plot in Figure 3 a comparison between our results and the isochrones of Lodato et al. (2017) for $M_{\text{disk}}/\dot{M}_{\text{acc}} = 10^4$, 10^5 , and 10^6 yr, and initial disk masses of 0.01, 0.1, and $1 M_\odot$. Results suggest that there is no correlation between the assumed age of the stars and the viscous timescales of the isochrones, and that our data can be reproduced by a variety of isochrones with different t_ν and initial disks conditions. We note that most of the sources cluster in the region between 10^5 and 10^6 yr and $M_{\text{disk},0}$ between 0.01 and $1 M_\odot$.

3.2. The $\dot{M}_{\text{acc}}-M_{\text{disk}}$ Evolution

The comparison between the Class I and Class II $\dot{M}_{\text{acc}}-M_{\text{disk}}$ distributions leads to the question: are our Class I sources going to produce a Lupus Class II population in 1 Myr? A positive

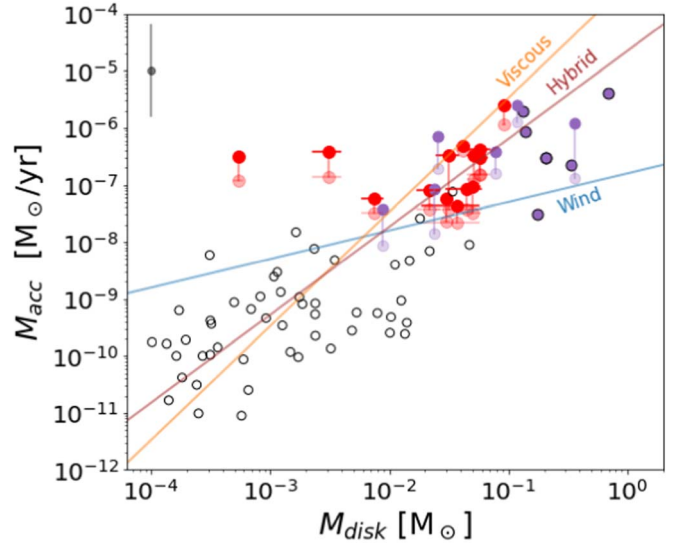


Figure 4. Mass accretion rate vs. disk dust mass. The symbols are the same as in Figure 1. The solid lines represent evolutionary tracks assuming different models: purely viscous (orange), a hybrid viscous and MHD wind (brown), and dominated by MHD wind (light blue).

answer to this question would imply not only that the disk is able to survive until the Class II stage, but also that the \dot{M}_{acc} and M_{disk} values are compatible with the Class II population ones.

In order to put the measured accretion rates and disk masses in the context of disk evolution models, we plot in Figure 4 evolutionary tracks of different evolution models, namely viscous evolution, pure disk wind evolution, and a hybrid case in which both modes of evolution are in place. Each of the models is briefly described below.

According to Lodato et al. (2017), the evolutionary track of a viscously evolving disk is prescribed as:

$$\dot{M}_{\text{acc}} = \frac{1}{2(2-\gamma)} \frac{M_0}{t_\nu} \left(\frac{M_{\text{disk}}}{M_0} \right)^{5-2\gamma}, \quad (3)$$

where M_0 is the initial disk mass, t_ν is the aforementioned viscous timescale, and γ is a factor depending on the value of the viscosity and the radius of the source. For γ we assume 1.5, following the value assumed by Lodato et al. (2017), where 1.5 is showed to be consistent with the minimum-mass solar nebula and a value between 1.2 and 2 is needed to reproduce the evolution of disks in Lupus. We set $M_0 = 1 M_\odot$ to match the presented samples.

Evolution of the disk under both an MHD disk wind and viscous effects (i.e., the hybrid model) follows the relation described by Tabone et al. (2021):

$$\dot{M}_{\text{acc}} = \dot{M}_{\text{acc},0} \left(\frac{M_{\text{disk}}}{M_0} \right)^{\frac{\psi+3+4\xi}{\psi+1+2\xi}}, \quad (4)$$

where $\dot{M}_{\text{acc},0}$ is the initial accretion rate, ψ is the ratio between the wind and turbulent torque, and ξ is the mass ejection index, which is a derivative of $\ln(\dot{M}_{\text{acc}})$ over $\ln(r)$, as defined by Ferreira & Pelletier (1995). Values of the parameters used to compare the model with our results on Figure 4 are $\psi = 3$ and $\xi = 0.1875$, following the prescription of Tabone et al. (2021), and $\dot{M}_{\text{acc},0} = 10^5$ yr is used to best fit the data. In a disk where accretion and mass-loss evolution is purely dependent on the

MHD wind, the relation can be parametrized as follows (Tabone et al. 2021):

$$\dot{M}_{\text{acc}} = \dot{M}_{\text{acc},0} \left(\frac{M_{\text{disk}}}{M_0} \right)^{1-\omega}, \quad (5)$$

where ω is an index that describes the dependence of the disk wind torque on the characteristic surface density. For the representative comparison we select intermediate values of $\omega = 0.5$ and $\dot{M}_{\text{acc},0} = 10^5 \text{ yr}$ to best fit the data. Tabone et al. (2021) showed that the slope of the evolutionary track changes when MHD disk wind effects are introduced. The slope becomes shallower for a disk wind with a magnetic field strength that decreases with time, up to becoming completely flat (i.e., a constant accretion rate with decreasing mass) for a constant magnetic field strength with disk evolution. The pure viscous model prescribed by Equation (3) is shown in Figure 4 (orange line), together with the evolutionary tracks of a hybrid model of a viscous and MHD disk wind (brown line), and another hybrid model where the MHD disk wind largely dominates the evolution (brown dashed line), reproduced using Equations (60) and 61 in Tabone et al. (2021), respectively. Figure 4 suggests that we can conclude that the pure viscous model does not describe well the transition between our Class I sample and the Lupus Class II YSOs, at least, not for protostars with disk masses $\ll 10^{-2} M_{\odot}$ and $> 0.1 M_{\odot}$. Also, the purely MHD disk wind evolution of the accretion disk seems unlikely to reproduce the evolution from Class I to Class II that we observe. But it is interesting to notice that the slope of the MHD wind model can reproduce the trend of the only Class I sample if it is shifted toward the top of the plot, i.e., by assuming higher \dot{M}_{acc} . However, the plot qualitatively suggests that the hybrid model can better represent both the Class I and II data distributions; therefore, some wind contribution should be included in the viscous evolution to best reproduce the observations.

Limitations of comparing our observational results with models lie in the following two reasons. First, these models do not investigate the earliest stages of star formation, in other words, the models of Lodato et al. (2017) and Tabone et al. (2021) both set the disk mass to a fixed value that dissipates with time as mass is accreted onto the forming star, while in the protostellar phase the disk mass is replenished by the envelope. Second, both the magnetic effects and the disk viscous timescale depend on environmental effects, and our sample is composed by Class I stars belonging to very different regions in the solar neighborhood. Naturally, observations of single star-forming clouds and models that include the earliest stages of disk formation are necessary to constrain further the disk wind and the viscous model. Also, the disk masses are highly uncertain, so obtaining disk masses at longer wavelengths, like the upcoming Band 1 of ALMA or the shortest VLA wavelengths, would improve this analysis. Moreover, the uncertainty on the protostars' aged propagates to the mass accretion rates, providing uncertainties larger than for the Class II PMS stars.

3.3. \dot{M}_{acc} versus M_{disk} Relation and Planet Formation

Assuming that planets form by accreting material onto planetesimals, and given some assumptions on the disk

structure and evolution, in the last decade many population synthesis models were developed to describe different kinds of produced exoplanetary systems (see Benz et al. 2014 for a review). In particular, the population synthesis of planet formation by Lubow & D'Angelo (2006) predicts a population of disks with greatly decreased accretion rates onto protostars due to the presence of gas giant planets. We do not see this population in the $\dot{M}_{\text{acc}} - M_{\text{disk}}$ plot, as Manara et al. (2019) found for CTTSs, showing that this effect is not present even in younger disks. It is unclear if those disks are massive enough to host gas giants or perhaps this effect is not present in general.

4. Summary and Conclusions

We presented for the first time in this letter the \dot{M}_{acc} versus M_{disk} plot populated with Class I YSOs, shifting to the protostellar stage the investigation of the disk's initial conditions, crucial for understanding star and planet formation. Our data show that younger sources present higher mass accretion rates, have more massive disks in general, and have "depletion times" (i.e., $M_{\text{disk}} - \dot{M}_{\text{acc}}$) faster than Class II YSOs, suggesting an evolutionary trend between Class I and II YSOs. We also measure higher \dot{M}_{acc} in Class I than in Class II with the same disk mass. Since our sample is limited to the brightest and, thus, older sources among Class I YSOs, we can consider our results as lower limits for Class I in general.

We fitted the $\dot{M}_{\text{acc}} - M_{\text{disk}}$ distribution of our Class I sample finding a slope flatter than the corresponding slope for Class II sources. But focusing only on the more massive disks, we found the Class I slope is in agreement with the Class II slope, suggesting that differences between the $\dot{M}_{\text{acc}} - M_{\text{disk}}$ distribution of Class I and II YSOs should be investigated for protostars whose disk masses are comparable with the typical Class II M_{disk} .

We tested our results with most recent viscous and MHD wind models. We tentatively speculate that our data can be described by the viscous model together with some contamination by MHD winds (hybrid model). However, we find no definitive conclusions about which of these models better represent our data. We associated this to the absence of an envelope feeding the disk in these models, and to the fact that even if our sample is analysed in an homogeneous way, it is affected by different environmental effects, since these protostars belong to different star-forming regions.

Uniform samples of Class I and Class II protostars with identical initial conditions, i.e., in the same star-forming region, and theoretical models which describe both stages are necessary to draw solid conclusions on the evolutionary path of YSOs and to be able to set the initial conditions for star and planet formation. While VLT/KMOS can be used efficiently for larger samples, JWST will deliver more sensitive information on photospheres with NIRSpect, and eventually enable investigations of the protostellar accretion rates for even more embedded sources with MIRI.

We thank the anonymous referee for the useful comments which improve this manuscript. This project has received funding from the European Research Council (ERC) under the European Union's Horizon 2020 Research & Innovation Programme under grant agreement No 716155 (SACCRED), and by the European Union under the European Union's Horizon Europe Research & Innovation Programme 101039452 (WANDA). Views and opinions expressed are

however those of the author(s) only and do not necessarily reflect those of the European Union or the European Research Council. Neither the European Union nor the granting authority can be held responsible for them. GR acknowledges support from the Netherlands Organisation for Scientific Research (NWO, program number 016.Veni.192.233) and from an STFC Ernest Rutherford Fellowship (grant number ST/T003855/1).

Software: astropy (Astropy Collaboration et al. 2013, 2018), astroquery, matplotlib.

Appendix The Sample

Table 1 lists the main properties of the protostars included in the analysis.

Table 1
List of Protostars' Properties

Name	Cloud	Distance	\dot{M}_{acc}	M_{dust}	ref.
(1)	(2)	pc (3)	M_{\odot}/yr (4)	M_{\oplus} (5)	(6)
IRS2	CrA	$160.5 \pm 1.8^{\text{a}}$	3×10^{-7}	693.8 ± 1.6	1, 4
IRS5a	CrA	$160.5 \pm 1.8^{\text{a}}$	3×10^{-8}	587.1 ± 2.1	1, 4
HH100IR	CrA	$160.5 \pm 1.8^{\text{a}}$	2×10^{-6}	443.5 ± 8.0	1, 4
HH 26 IRS	L1630	450	8.5×10^{-7}	468.7 ± 18.1	2, 5
HH 34 IRS	L1641	460	41.1×10^{-7}	2282.7 ± 67.7	2, 5
HH 46 IRS	Bok globule	450	2.2×10^{-7}	1126.8 ± 14.5	2, 6
2MASSJ03283968 + 3117321	NGC 1333	$293 \pm 22^{\text{b}}$	$(1.4 - 8.3) \times 10^{-8}$	12.8 ± 0.8	3, 6
2MASSJ03285842 + 3122175	NGC 1333	$293 \pm 22^{\text{b}}$	$(19 - 70) \times 10^{-8}$	11.3 ± 0.6	3, 6
2MASSJ03290149 + 3120208	NGC 1333	$293 \pm 22^{\text{b}}$	$(16 - 38) \times 10^{-8}$	7.7 ± 2.2	3, 6
SVS 13 (V512 Per) [†]	NGC 1333	$293 \pm 22^{\text{b}}$	$(19 - 220) \times 10^{-8}$	969.7 ± 15.5	3, 7
LAL96 213	NGC 1333	$293 \pm 22^{\text{b}}$	$(13 - 120) \times 10^{-8}$	318.5 ± 0.9	3, 6
2MASSJ03292003 + 3124076	NGC 1333	$293 \pm 22^{\text{b}}$	$(0.8 - 3.6) \times 10^{-8}$	3.8 ± 1.6	3, 8
CG2010IRAS032203035N	Per-IC348	$219.8 \pm 16.2^{\text{a}}$	$(3.2 - 9.3) \times 10^{-8}$	167 ± 25	this work, 7
2MASSJ033312843121241	Per-IC348	$319.5 \pm 23.7^{\text{a}}$	$(1.5 - 3.0) \times 10^{-7}$	190 ± 28	this work, 6
BHS98MHO1	Tau-L1495	$134.0 \pm 7.0^{\text{a}}$	$(1.2 - 3.3) \times 10^{-7}$	171 ± 18	this work, 9
BHS98MHO2	Tau-L1495	$131.0 \pm 2.9^{\text{a}}$	$(2.3 - 5.9) \times 10^{-8}$	100.5 ± 4.5	this work, 9
IRAS041692702	Tau-L1495	$129.5 \pm 12.9^{\text{c}}$	$(3.6 - 8.3) \times 10^{-8}$	147 ± 47	this work, 10
VFSTau	Tau-Aur	$133.9 \pm 2.4^{\text{d}}$	$(1.2 - 3.2) \times 10^{-7}$	1.79 ± 0.13	this work, 11
2MASSJ042200692657324	Tau-Aur	$133.9 \pm 2.4^{\text{d}}$	$(3.9 - 4.8) \times 10^{-7}$	139 ± 15	this work, 12
IRAS042952251	Tau-L1546	$160.76 \pm 16.1^{\text{c}}$	$(2.1 - 4.4) \times 10^{-8}$	125 ± 62	this work, 10
IRAS043812540	Tau-L1527	$141.8 \pm 1.4^{\text{c}}$	$(3.2 - 5.9) \times 10^{-8}$	24.6 ± 4.9	this work, 13
Parenago2649	ONC A	$398.5 \pm 2.5^{\text{a}}$	$(0.4 - 3.3) \times 10^{-7}$	105 ± 21	this work, 14
2MASSJ054050590805487	ONC A	$440 \pm 44^{\text{e}}$	$(3.6 - 8.1) \times 10^{-8}$	72 ± 15	this work, 15
2MASSJ054049910806084	ONC A	$440 \pm 44^{\text{e}}$	$(1.3 - 3.7) \times 10^{-7}$	10.2 ± 2.7	this work, 15
IRAS054050117	ONC B	$420 \pm 42^{\text{e}}$	$(1.5 - 4.2) \times 10^{-7}$	191 ± 38	this work, 15
VSCrA	CrA	$160.5 \pm 1.8^{\text{a}}$	$(0.5 - 2.1) \times 10^{-8}$	306.7 ± 6.9	this work, 4

Notes.

^a Parallax distance with Gaia EDR3 direct match (Gaia Collaboration et al. 2021), Distance to the region (error is set to 10% if not stated in literature).

^b Ortiz-León et al. (2018).






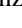


^c Krolkowski et al. (2021)

^d Assumed to be the same as FS TauA where Gaia EDR3 is available.

^e Tobin et al. (2020).

References: 1 - Nisini et al. (2005b), 2 - Antonucci et al. (2008), 3 - Fiorellino et al. (2021), 4 - ALMA#2019.1.01792.S, 5 - Tobin et al. (2020), 6 - Tychoniec et al (2020), 7 - Tobin et al. (2018), 8 - Yang et al. (2021), 9 - Akeson & Jensen (2014), 10 - Sheehan & Eisner (2017), 11 - Akeson et al. (2019), 12 - Villenave et al. (2020), 13 - van't Hoff et al (2020), 14 - ALMA#2019.1.01813.S, 15 - Tobin et al. (2020). The mass accretion rates correspond to the range of values inferred assuming an age varying from the birthline to 1 Myr.

ORCID iDs

Eleonora Fiorellino  <https://orcid.org/0000-0002-5261-6216>
 Łukasz Tychoniec  <https://orcid.org/0000-0002-9470-2358>
 Carlo F. Manara  <https://orcid.org/0000-0003-3562-262X>
 Giovanni Rosotti  <https://orcid.org/0000-0003-4853-5736>
 Simone Antonucci  <https://orcid.org/0000-0002-0666-3847>
 Fernando Cruz-Sáenz de Miera  <https://orcid.org/0000-0002-4283-2185>
 Ágnes Kóspál  <https://orcid.org/0000-0001-7157-6275>
 Brunella Nisini  <https://orcid.org/0000-0002-9190-0113>

References

- Akeson, R. L., & Jensen, E. L. N. 2014, *ApJ*, **784**, 62
 Akeson, R. L., Jensen, E. L. N., Carpenter, J., et al. 2019, *ApJ*, **872**, 158
 Alcalá, J. M., Manara, C. F., Natta, A., et al. 2017, *A&A*, **600**, A20
 Antonucci, S., Nisini, B., Giannini, T., & Lorenzetti, D. 2008, *A&A*, **479**, 503
 Astropy Collaboration, Price-Whelan, A. M., Sipőcz, B. M., et al. 2018, *AJ*, **156**, 123
 Astropy Collaboration, Robitaille, T. P., Tollerud, E. J., et al. 2013, *A&A*, **558**, A33
 Benz, W., Ida, S., Alibert, Y., Lin, D., & Mordasini, C. 2014, in *Protostars and Planets VI*, ed. H. Beuther et al. (Tucson, AZ: Univ. Arizona Press), 691
 Connelley, M. S., & Greene, T. P. 2010, *AJ*, **140**, 1214
 Doppmann, G. W., Greene, T. P., Covey, K. R., & Lada, C. J. 2005, *AJ*, **130**, 1145
 Dullemond, C. P., Natta, A., & Testi, L. 2006, *ApJL*, **645**, L69
 Dunham, M. M., Stutz, A. M., Allen, L. E., et al. 2014, in *Protostars and Planets VI*, ed. H. Beuther et al. (Tucson, AZ: Univ. Arizona Press), 195
 Enoch, M. L., Evans, N. J. I., Sargent, A. I., & Glenn, J. 2009, *ApJ*, **692**, 973
 Ferreira, J., & Pelletier, G. 1995, *A&A*, **295**, 807
 Fiorellino, E., Manara, C. F., Nisini, B., et al. 2021, *A&A*, **650**, A43
 Gaia Collaboration, Brown, A. G. A., Vallenari, A., et al. 2021, *A&A*, **649**, A1
 Hartmann, L., Calvet, N., Gullbring, E., & D'Alessio, P. 1998, *ApJ*, **495**, 385
 Hartmann, L., Herczeg, G., & Calvet, N. 2016, *ARA&A*, **54**, 135
 Hennebelle, P., Commerçon, B., Lee, Y.-N., & Charnoz, S. 2020, *A&A*, **635**, A67
 Hueso, R., & Guillot, T. 2005, *A&A*, **442**, 703
 Kelly, B. C. 2007, *ApJ*, **665**, 1489
 Krolikowski, D. M., Kraus, A. L., & Rizzuto, A. C. 2021, *AJ*, **162**, 110
 Laos, S., Greene, T. P., Najita, J. R., & Stassun, K. G. 2021, *ApJ*, **921**, 110
 Lodato, G., Scardoni, C. E., Manara, C. F., & Testi, L. 2017, *MNRAS*, **472**, 4700
 Lorenzetti, D., Antonucci, S., Giannini, T., et al. 2013, *Ap&SS*, **343**, 535
 Lubow, S. H., & D'Angelo, G. 2006, *ApJ*, **641**, 526
 Manara, C. F., Ansdell, M., Rosotti, G. P., et al. 2022, arXiv:2203.09930
 Manara, C. F., Mordasini, C., Testi, L., et al. 2019, *A&A*, **631**, L2
 Manara, C. F., Natta, A., Rosotti, G. P., et al. 2020, *A&A*, **639**, A58
 Manara, C. F., Rosotti, G., Testi, L., et al. 2016, *A&A*, **591**, L3
 Maury, A. J., André, P., Testi, L., et al. 2019, *A&A*, **621**, A76
 Miotello, A., Kamp, I., Birnstiel, T., Cleeves, L. I., & Kataoka, A. 2022, arXiv:2203.09818
 Muzerolle, J., Hartmann, L., & Calvet, N. 1998, *AJ*, **116**, 2965
 Natta, A., Testi, L., Randich, S., & Muzerolle, J. 2005, *MmSAI*, **76**, 343
 Nisini, B., Antonucci, S., Giannini, T., & Lorenzetti, D. 2005a, *A&A*, **429**, 543
 Nisini, B., Bacciotti, F., Giannini, T., et al. 2005b, *A&A*, **441**, 159
 Ortiz-León, G. N., Loinard, L., Dzib, S. A., et al. 2018, *ApJ*, **865**, 73
 Ossenkopf, V., & Henning, T. 1994, *A&A*, **291**, 943
 Palla, F., & Stahler, S. W. 1990, *ApJL*, **360**, L47
 Rosotti, G. P., Clarke, C. J., Manara, C. F., & Facchini, S. 2017, *MNRAS*, **468**, 1631
 Sheehan, P. D., & Eisner, J. A. 2017, *ApJ*, **851**, 45
 Sheehan, P. D., Tobin, J. J., Looney, L. W., & Megeath, S. T. 2022, *ApJ*, **929**, 76
 Tabone, B., Rosotti, G. P., Cridland, A. J., Armitage, P. J., & Lodato, G. 2021, *MNRAS*, **512**, 2290
 Tobin, J. J., Looney, L. W., Li, Z.-Y., et al. 2018, *ApJ*, **867**, 43
 Tobin, J. J., Sheehan, P. D., Megeath, S. T., et al. 2020, *ApJ*, **890**, 130
 Tychoniec, Ł., Manara, C. F., Rosotti, G. P., et al. 2020, *A&A*, **640**, A19
 van 't Hoff, M. L. R., Harsono, D., Tobin, J. J., et al. 2020, *ApJ*, **901**, 166
 Villenave, M., Ménard, F., Dent, W. R. F., et al. 2020, *A&A*, **642**, A164
 White, R. J., & Hillenbrand, L. A. 2004, *ApJ*, **616**, 998
 Williams, J. P., Cieza, L., Hales, A., et al. 2019, *ApJL*, **875**, L9
 Yang, Y.-L., Sakai, N., Zhang, Y., et al. 2021, *ApJ*, **910**, 20
 Zhao, B., Tomida, K., Hennebelle, P., et al. 2020, *SSRv*, **216**, 43
 Zhu, Z., Zhang, S., Jiang, Y.-F., et al. 2019, *ApJL*, **877**, L18